

Article

Battery State-Of-Charge Estimation Based on a Dual Unscented Kalman Filter and Fractional Variable-Order Model

Ming Cai, Weijie Chen and Xiaojun Tan *

School of Engineering, Sun Yat-sen University, 135 Xingang Xi Road, Haizhu District, Guangzhou 510275, China; caiming@mail.sysu.edu.cn (M.C.); cwjvictor@foxmail.com (W.C.)

* Correspondence: tanxj@mail.sysu.edu.cn; Tel.: +86-138-0888-8016

Received: 14 September 2017; Accepted: 3 October 2017; Published: 12 October 2017

Abstract: State-of-charge (SOC) estimation is essential for the safe and effective utilization of lithium-ion batteries. As the SOC cannot be directly measured by sensors, an accurate battery model and a corresponding estimation method is needed. Compared with electrochemical models, the equivalent circuit models are widely used due to their simplicity and feasibility. However, such integer order-based models are not sufficient to simulate the key behavior of the battery, and therefore, their accuracy is limited. In this paper, a new model with fractional order elements is presented. The fractional order values are adaptively updated over time. For battery SOC estimation, an unscented fractional Kalman filter (UFKF) is employed based on the proposed model. Furthermore, a dual estimation scheme is designed to estimate the variable orders simultaneously. The accuracy of the proposed model is verified under different dynamic profiles, and the experimental results indicate the stability and accuracy of the estimation method.

Keywords: state-of-charge; unscented Kalman filter; fractional order modeling; online estimation; lithium-ion battery

1. Introduction

In recent years electrified vehicles, including battery electric vehicles (BEVs), hybrid electric vehicles (HEVs) and plug-in hybrid electric vehicles (PHEVs), have undergone considerable development as an alternative solution to replace traditional internal combustion engine (ICE) vehicles [1]. To meet the power and range requirement in a limited space, lithium-ion batteries have been widely used in electrified vehicles due to their high energy density and excellent power abilities. In practical applications, the single battery cells are often series and parallel connected to form a battery system, which requires a battery management system (BMS) to monitor the states of the cells to ensure safe and efficient operation.

Among the states that should be detected by the BMS, the state-of-charge (SOC) is of great importance [2]. In terms of safety, the SOC should be accurately estimated to avoid over-charge and over-discharge. In terms of efficiency, strategies for charging, balancing and energy control are essentially dependent on the SOC. Furthermore, in terms of practicality, the SOC provides the user with information regarding the remaining range, thus reducing the drive anxiety. However, the SOC cannot be measured directly and should be estimated by other measurable parameters through a specific model.

Several estimation methods have been proposed in the literature [3–5]. The Coulomb counting method is the most straightforward and is easily implemented. However, it has some drawbacks, including the inaccuracy of determining the initial SOC, the accumulated error over time and the uncertainty in the Coulomb efficiency. Some measurable parameters, such as the open circuit

voltage (OCV) and internal resistance, can be used for precise SOC estimation; however, either long wait times to achieve a stabilized status or special equipment to perform the tests are required, so these methods are not suitable for real time estimation. In addition, purely data-driven algorithms, such as fuzzy logic [6,7], artificial neuronal networks [8,9] and support vector machines [10,11], are applied to SOC estimation. However, these methods require huge data sets for training and are difficult to implement.

Model-based estimation methods have gained much popularity in the literature recently. The most commonly used battery models can be classified into electrochemical models and equivalent circuit models [12–14]. The electrochemical models [15–18] focus on the physical principles in the battery using a large number of parameters as well as partial differential equations. These models can simulate the battery behavior precisely. However, the heavy computational burden and high implementation complexity limit their application. The equivalent circuit models [19–21] use basic electric components, such as resistors and capacitors, to simulate the characteristics of a battery. These models have fewer parameters with a higher computational efficiency and are thus suitable for on-board estimation. Nevertheless, the integer order components used in these models are not sufficient to describe the highly nonlinear effects of the battery, which limits the accuracy.

In recent years, fractional order calculus (FOC) has been widely used in various fields [22,23] and is applied in battery modeling. Wu et al. [24] designed an FOC-based state space model, but the differentiation order was fixed to 0.5 and 1. In [25–27], fractional order models with free differentiation orders were proposed. However, the order values are obtained by offline methods and are not adaptive to changing conditions. For SOC estimation, Zhong et al. [28] implemented a sliding mode observer to estimate states in real time for fractional order systems, but the parameters remain fixed during the working cycle. In [29–31], the extended fractional Kalman filter (EFKF) was employed to achieve state estimation where the system process noise and measurement noise can be filtered. However, since the battery model is highly nonlinear, the Taylor expansion-based linearization process may result in large approximation errors.

In this paper, a battery SOC estimation method based on a dual unscented Kalman filter and fractional variable-order model is proposed. First, the merits of wider parameter ranges and better hereditary property descriptions of fractional order calculus are adopted for battery modeling, and the fractional orders are free to adapt to uncertain dynamics. Second, the unscented Kalman filter is modified to suit the fractional system and is employed to achieve more accurate SOC estimation. Third, the dual estimation scheme is designed to identify order values online. The remainder of the paper is organized as follows. Section 2 introduces the definition of fractional order calculus and the structure of the proposed model. The unscented fractional Kalman filter (UFKF) is designed for the state estimation in Section 3. The dual filter scheme for simultaneous order estimation is depicted in Section 4. The model accuracy and SOC estimation results are presented in Section 5. In Section 6, some conclusions are drawn.

2. Fractional Order Calculus and Fractional Battery Model

The concept of fractional order calculus has been widely applied in engineering and research areas, such as permanent magnet synchronous motors [32], proportional–integral–derivative (PID) controllers [33], heat transfer models [34], and others. In general, systems having long memory, hereditary properties and dynamical processes can be more sufficiently modeled by FOC [35].

According to the methods used in the generalization of integer-order calculus, FOC can be defined in several different forms [36,37]. In this paper, the Grünwald–Letnikov definition [36] is used for discretization of the continuous fractional order equations. The α -order FOC is defined as:

$$\mathfrak{D}^{\alpha} x_k = \frac{1}{T_s^{\alpha}} \sum_{j=0}^k (-1)^j \binom{\alpha}{j} x_{k-j} \quad (1)$$

$$\binom{\alpha}{j} = \begin{cases} 1 & j = 0 \\ \frac{\alpha(\alpha-1)\dots(\alpha-(j-1))}{j!} & j > 0 \end{cases} \quad (2)$$

where \mathfrak{D} is the differential operator, α is the differential order value, T_s is the sample time and k is the current time step. Here, the fractional order α is assumed to be constant. For the case of variable orders, there are several ways to extend this definition. In this paper, the A-type variable-order FOC in [38] is adopted due to its simplicity and is defined as:

$$\mathfrak{D}^{\alpha_k} x_k = \frac{1}{T_s^{\alpha_k}} \sum_{j=0}^k (-1)^j \binom{\alpha_k}{j} x_{k-j} \quad (3)$$

where the constant order α in (1) is replaced by an adaptable order α_k .

For batteries, it has been proven in the literature that many phenomena that occur in them, such as mass transport [39] and the double-layer effect [40], can be well characterized by FOC. The fractional behaviors of the battery can be indicated using electrochemical impedance spectroscopy (EIS) analysis, which is a useful method to explore battery properties. The typical impedance spectrum plot (Nyquist plot) for lithium-ion batteries can be divided into three sections [27]. In the high frequency section, the battery can be simply expressed by an ohmic resistor. In the middle frequency section, the Nyquist plot is a depressed semicircle, and the behavior of the battery can be represented by a constant phase element (CPE) in parallel with a transfer resistance. The CPE is a special element that follows a partially capacitive and resistive behavior [26]. The parallel combination of the CPE and the resistance is also called the “element that yields an arc in the Z plane (ZARC) element” in some studies [40]. In the low frequency section, the battery internal dynamics can be described by a parallel RC circuit with a Warburg element [41,42] or a single ZARC element [27,28]. According to the analysis above, the battery model can be constructed as in Figure 1.

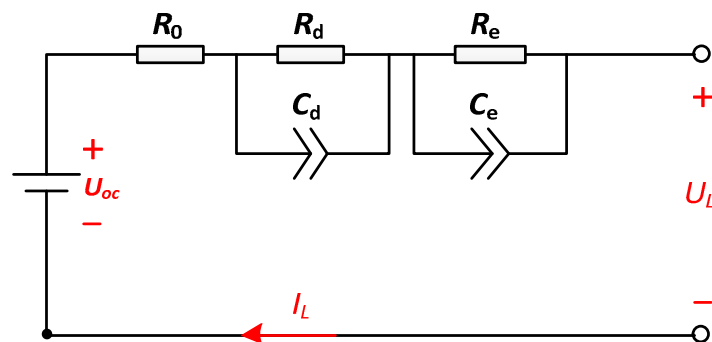


Figure 1. Schematic diagram of the fractional order battery model.

As shown in Figure 1, the fractional battery model consists of a voltage source, an ohmic resistor and two ZARC elements. The mathematical relationship between the current input and the terminal voltage output of the proposed model can be given as:

$$U_L = U_{oc} - I_L R_0 - U_d - U_e \quad (4)$$

$$\mathfrak{D}^{\alpha_d} U_d = \frac{I_L}{C_d} - \frac{U_d}{C_d R_d} \quad (5)$$

$$\mathfrak{D}^{\alpha_e} U_e = \frac{I_L}{C_e} - \frac{U_e}{C_e R_e} \quad (6)$$

where U_{oc} denotes the open circuit voltage, I_L is the load current, U_L represents the terminal voltage, U_d and U_e denote voltages across the two ZARC elements, which indicate the concentration polarization and electrochemical polarization effects of the battery [28], R_0 , R_d , C_d , R_e and C_e represent

the ohmic resistance, concentration polarization resistance and capacitance, and electrochemical polarization resistance and capacitance, and α_d and α_e are the differentiation orders of the two CPE elements, which are both within (0, 1). When $\alpha_d = \alpha_e = 1$, the model is equivalent to the classic second-order RC circuit model.

By applying the A-type variable-order FOC definition in (3), Equation (5) can be discretized as:

$$\frac{1}{T_s^{\alpha_{d,k}}} \sum_{j=0}^k (-1)^j \binom{\alpha_{d,k}}{j} U_{d,k-j} = \frac{I_{L,k-1}}{C_d} - \frac{U_{d,k-1}}{C_d R_d} \quad (7)$$

It should be noted that the upper bound of the sum of the past states is set as the current time step k according to the definition to preserve the complete information of the entire past. However, the computation burden is too heavy and is impractical to implement. To reduce the model complexity, the summing upper bound can be set as a fixed number, where only N_s points from the recent past are used. Then, $U_{d,k}$ can be solved as:

$$U_{d,k} = \left(\alpha_{d,k} - \frac{T_s^{\alpha_{d,k}}}{C_d R_d} \right) U_{d,k-1} + T_s^{\alpha_{d,k}} \frac{I_{L,k-1}}{C_d} - \sum_{j=2}^{N_s} (-1)^j \binom{\alpha_{d,k}}{j} U_{d,k-j} \quad (8)$$

Then, $U_{e,k}$ can be deduced in the same way. According to the definition of the SOC, one can acquire:

$$z_k = z_{k-1} - \frac{I_{L,k} \eta}{Q_N} \quad (9)$$

where z denotes the battery SOC, η is the Coulomb efficiency and Q_N is the battery nominal capacity.

Then, the state space format of the proposed fractional order model can be expressed as:

$$x_k = A_k x_{k-1} + B_k u_{k-1} - \sum_{j=2}^{N_s} (-1)^j \gamma_{j,k} x_{k-j} \quad (10)$$

$$y_k = h(x_k, u_k) = ocv(x_{3,k}) - u_k R_o - x_{1,k} - x_{2,k} \quad (11)$$

where $x_k = [u_{d,k}, u_{e,k}, z_k]^T$, $y_k = U_{L,k}$, $u_k = I_{L,k}$, $A_k = \begin{bmatrix} \alpha_{d,k} - \frac{T_s^{\alpha_{d,k}}}{C_d R_d} & 0 & 0 \\ 0 & \alpha_{e,k} - \frac{T_s^{\alpha_{e,k}}}{C_e R_e} & 0 \\ 0 & 0 & 1 \end{bmatrix}$,

$B_k = \left[\frac{T_s^{\alpha_{d,k}}}{C_d}, \frac{T_s^{\alpha_{e,k}}}{C_e}, -\frac{\eta}{Q_N} \right]^T$, $\gamma_{j,k} = \text{diag} \left\{ \binom{\alpha_{d,k}}{j}, \binom{\alpha_{e,k}}{j}, \binom{1}{j} \right\}$, and ocv denotes the nonlinear relationship between the battery SOC and the open circuit voltage. For simplicity, the sample time T_s and the Coulomb efficiency η are both set to be 1 in this paper.

3. State Estimation Using an Unscented Fractional Kalman Filter

As stated above, the conventional unscented Kalman filter is not directly applicable for fractional order systems, and thus should be extended [43]. In addition, such an algorithm should be further modified to suit the cases where the fractional orders may change with time. In this paper, based on the definition in (3), an unscented fractional Kalman filter for variable-order systems is implemented.

Consider the nonlinear fractional order discrete state space model given by:

$$\mathfrak{D}^{\alpha_k} x_k = f_k(x_{k-1}, u_{k-1}) + w_k \quad (12)$$

$$y_k = h_k(x_k, u_k) + v_k \quad (13)$$

where x denotes the system state to be estimated, u denotes the system input, y is the system output, $f(x, u)$ is the state transition function, $h(x, u)$ is the measurement function, and w and v are zero-mean Gaussian process noise with variance Q and measurement noise with variance R , respectively.

Calculate the weighting constants:

$$W_0^{(m)} = \lambda / (n + \lambda) \quad (14)$$

$$W_0^{(c)} = W_0^{(m)} + (1 - \alpha^2 + \beta) \quad (15)$$

$$W_i^{(m)} = W_i^{(c)} = 1/2(n + \lambda) \quad (16)$$

where n is the dimension of the state vector, and $\lambda = \alpha^2(n + \kappa) - n$, with $10^{-2} \leq \alpha \leq 1$ being the scaling parameter and $\kappa = 3 - n$ being the tuning parameter. Note that the constant α here is different from the fractional order α_k . β incorporates prior knowledge, and for the Gaussian distribution, $\beta = 2$.

Then, the UFKF can be summarized as follows:

Initialization: for $k = 0$, set

$$\hat{x}_{0|0} = E[x_0] \quad (17)$$

$$P_{0|0} = E[(x_0 - \hat{x}_{0|0})(x_0 - \hat{x}_{0|0})^T] \quad (18)$$

Computation: for $k = 1, 2, \dots$, compute the following:

(a) Sigma points generation

$$\chi_{0,k-1|k-1} = \hat{x}_{k-1|k-1} \quad (19)$$

$$\chi_{i,k-1|k-1} = \hat{x}_{k-1|k-1} + \left(\sqrt{(n + \lambda)P_{k-1|k-1}} \right)_i, \quad i = 1, \dots, n \quad (20)$$

$$\chi_{i,k-1|k-1} = \hat{x}_{k-1|k-1} - \left(\sqrt{(n + \lambda)P_{k-1|k-1}} \right)_i, \quad i = n + 1, \dots, 2n \quad (21)$$

(b) State estimation time update

$$\mathfrak{D}^{\alpha_k} \hat{x}_{k|k-1} = \sum_{i=0}^{2n} W_i^{(m)} f_k(\chi_{i,k-1|k-1}, u_{k-1}) \quad (22)$$

$$\hat{x}_{k|k-1} = \mathfrak{D}^{\alpha_k} \hat{x}_{k|k-1} - \sum_{j=1}^{N_s} (-1)^j \gamma_{j,k-1} \hat{x}_{k-j|k-j} \quad (23)$$

(c) State error covariance time update

$$P_{k|k-1}^{\Delta\Delta} = \sum_{i=0}^{2n} W_i^{(c)} (f_k(\chi_{i,k-1|k-1}, u_{k-1}) - \mathfrak{D}^{\alpha_k} \hat{x}_{k|k-1}) \times (f_k(\chi_{i,k-1|k-1}, u_{k-1}) - \mathfrak{D}^{\alpha_k} \hat{x}_{k|k-1})^T + Q_{k-1} \quad (24)$$

$$P_{k|k-1}^{x\Delta} = \sum_{i=0}^{2n} W_i^{(c)} (\chi_{i,k-1|k-1} - \hat{x}_{k-1|k-1}) \times (f_k(\chi_{i,k-1|k-1}, u_{k-1}) - \mathfrak{D}^{\alpha_k} \hat{x}_{k|k-1})^T \quad (25)$$

$$P_{k|k-1} = P_{k|k-1}^{\Delta\Delta} + \gamma_{1,k-1} P_{k|k-1}^{x\Delta} + P_{k|k-1}^{\Delta x} \gamma_{1,k-1} + \sum_{j=1}^k \gamma_{j,k-1} P_{k-j|k-j} \gamma_{j,k-1} \quad (26)$$

(d) Output update

$$\chi_{i,k|k-1} = f_k(\chi_{i,k-1|k-1}, u_{k-1}) - \sum_{j=1}^{N_s} (-1)^j \gamma_{j,k-1} \hat{x}_{k-j|k-j} \quad (27)$$

$$\hat{y}_{k|k-1} = \sum_{i=0}^{2n} W_i^{(m)} h_k(\chi_{i,k|k-1}) \quad (28)$$

(e) State estimate measurement update

$$P_{k|k-1}^y = \sum_{i=0}^{2n} W_i^{(c)} (h_k(\chi_{i,k|k-1}) - \hat{y}_{k|k-1}) \times (h_k(\chi_{i,k|k-1}) - \hat{y}_{k|k-1})^T \quad (29)$$

$$P_{k|k-1}^{xy} = \sum_{i=0}^{2n} W_i^{(c)} (\chi_{i,k|k-1} - \hat{x}_{k|k-1}) \times (h_k(\chi_{i,k|k-1}) - \hat{y}_{k|k-1})^T \quad (30)$$

$$L_k = P_{k|k-1}^{xy} (P_{k|k-1}^y)^{-1} \quad (31)$$

$$\hat{x}_{k|k} = \hat{x}_{k|k-1} + L_k (y_k - \hat{y}_{k|k-1}) \quad (32)$$

(f) State error covariance measurement update

$$P_{k|k} = P_{k|k-1} - L_k P_{k|k-1}^y L_k^T \quad (33)$$

First, the filter is initialized according to the best estimation of the state and error covariance. Then, several sigma points are generated to approximate state estimates. Next, the state is updated through the transition function, and the state error covariance is calculated. Then, the system output is approximated using the transformed sigma points. After that, the posteriori state is corrected with the system estimation and measurement information, and finally, the error covariance is updated. The process above is repeated at each time step, and therefore, the system state is online estimated.

4. Fractional Order Estimation Using a Dual Filter

The parameters in the battery model may be influenced by many factors, such as temperature, battery SOC, capacity degradation, and others. To ensure the model accuracy under various operational conditions, the online parameter estimation should be carefully addressed. The use of a dual Kalman filter is an efficient approach to estimate the system states and model parameters simultaneously [44,45]. However, to the author's knowledge, such a method has not been investigated for FOC-based models, especially for order identification. Since the fractional order values have a remarkable impact on the fractional battery model [46], in this paper, the dual unscented fractional Kalman filter is proposed to update the orders in real time.

Generally, the dual estimator addresses parameters that can be integrated in the state transition function in the form of $f(x, u, \theta)$. However, as shown in (12), the fractional orders cannot be included directly into the transition function, and thus, the corresponding estimator should be specially designed [38]. The unscented fractional Kalman filter for variable order estimation can be depicted as follows.

Initialization: for $k = 0$, set

$$\hat{\alpha}_{0|0} = E[x_0] \quad (34)$$

$$P_{0|0}^\omega = E[(\alpha_0 - \hat{\alpha}_{0|0})(\alpha_0 - \hat{\alpha}_{0|0})^T] \quad (35)$$

where P^ω denotes the error covariance of the order.

Computation: for $k = 1, 2 \dots$, compute the following:

(a) Sigma points generation

$$\mathcal{W}_{0,k-1|k-1} = \hat{\alpha}_{k-1|k-1} \quad (36)$$

$$\mathcal{W}_{i,k-1|k-1} = \hat{\alpha}_{k-1|k-1} + \left(\sqrt{(n+\lambda)(P_{k-1|k-1}^\omega + Q_{k-1}^\omega)} \right)_i, \quad i = 1, \dots, n \quad (37)$$

$$\mathcal{W}_{i,k-1|k-1} = \hat{\alpha}_{k-1|k-1} - \left(\sqrt{(n+\lambda)(P_{k-1|k-1}^\omega + Q_{k-1}^\omega)} \right)_i, \quad i = n+1, \dots, 2n \quad (38)$$

where Q^ω denotes the covariance of the order noise.

(b) Order estimation time and measurement update

$$\hat{\alpha}_{k|k-1} = \sum_{i=0}^{2n} W_i^{(m)} \mathcal{W}_{i,k-1|k-1} \quad (39)$$

$$\chi_{i,k|k-1}^\omega = f_k(\hat{x}_{k|k-1}, u_{k-1}) - \sum_{j=1}^{N_s} (-1)^j \binom{\mathcal{W}_{i,k-1|k-1}}{j} \hat{x}_{k-j|k-j} \quad (40)$$

$$y_{k|k-1}^\omega = \sum_{i=0}^{2n} W_i^{(m)} h_k(\chi_{i,k|k-1}^\omega) \quad (41)$$

$$P_{k|k-1}^{y\omega} = \sum_{i=0}^{2n} W_i^{(c)} \left(h_k(\chi_{i,k|k-1}^\omega) - y_{k|k-1}^\omega \right) \times \left(h_k(\chi_{i,k|k-1}^\omega) - y_{k|k-1}^\omega \right)^T + R^\omega \quad (42)$$

where R^ω denotes the covariance of the measurement noise caused by the uncertain order variation.

$$P_{k|k-1}^{xy\omega} = \sum_{i=0}^{2n} W_i^{(c)} \left(\mathcal{W}_{i,k-1|k-1} - \hat{\alpha}_{k|k-1} \right) \times \left(h_k(\chi_{i,k|k-1}^\omega) - y_{k|k-1}^\omega \right)^T \quad (43)$$

$$L_k^\omega = P_{k|k-1}^{xy\omega} \left(P_{k|k-1}^{y\omega} \right)^{-1} \quad (44)$$

$$\hat{\alpha}_{k|k} = \hat{\alpha}_{k|k-1} + L_k^\omega \left(y_k - y_{k|k-1}^\omega \right) \quad (45)$$

(c) Order error covariance measurement update

$$P_{k|k}^\omega = P_{k|k-1}^\omega - L_k^\omega P_{k|k-1}^{y\omega} L_k^{\omega T} \quad (46)$$

$$Q_k^\omega = (1-\delta)Q_{k-1}^\omega + \delta L_k^\omega \left(y_k - y_{k|k-1}^\omega \right) \left(y_k - y_{k|k-1}^\omega \right)^T \left(L_k^\omega \right)^T \quad (47)$$

where $\delta \in (0, 1]$ is the forgetting factor.

The total scheme of the dual unscented fractional Kalman filter for coestimation of the state and variable order is shown in Figure 2. The two separate filters run in parallel at each time step with information exchange. The state filter adapts the states using the best order estimates from the previous time step, while the other filter adapts the order using the state prediction from the current time step. In this way, the values of states and model orders are optimally estimated to adapt to the changing operational conditions.

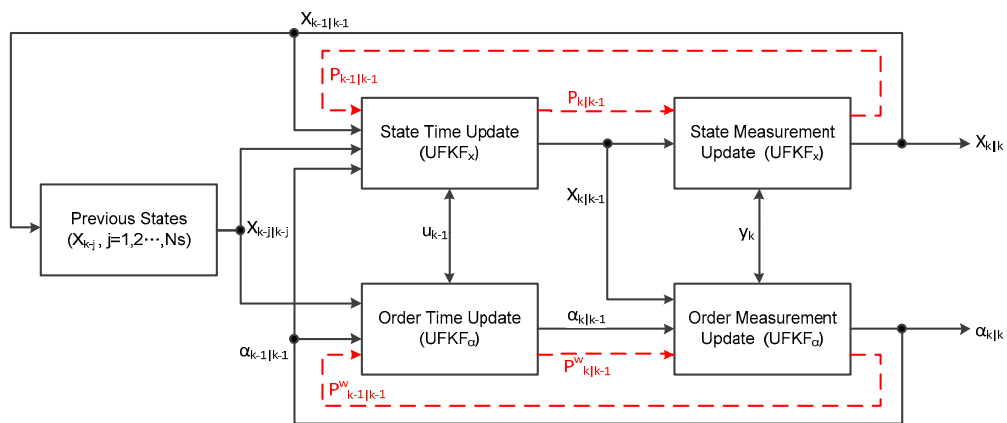


Figure 2. Block diagram of the dual estimation in the fractional order system. Solid lines denote state and order signal flow, and dashed red lines denote error covariance signal flow.

5. Experiments and Validations

5.1. Experimental Setup

Experiments are performed to evaluate the performance of the proposed method under real application conditions. A test bench is built consisting of an Arbin battery testing system BT2000 for voltammetry measurements, a programmable thermal chamber for temperature control and a host computer for data recording, as shown in Figure 3. The cylindrical Li-ion cell from LG (LGDBMG11865) with a nominal capacity of 2.9 Ah and a nominal voltage of 3.7 V is used for the tests.

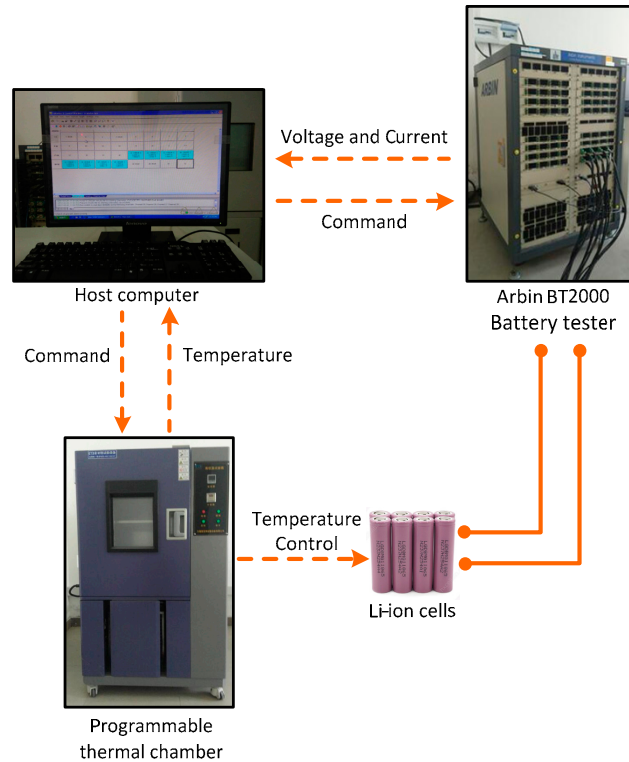


Figure 3. Diagram of the battery test bench.

The experiment schedule starts with the static capacity test at the temperature $T = 25$. Then, the hybrid pulse power characterization (HPPC) test is conducted to acquire the offline parameters. After that, the federal urban dynamic schedule (FUDS) and dynamic stress test (DST) are conducted to simulate real driving conditions.

5.2. Static Capacity and HPPC Test

The static capacity test is designed to determine the actual capacity of the cell. First, the cell is fully charged in a constant current, constant voltage mode, where the constant current is at a rate of $C/3$, and the constant voltage is the charge limit voltage of the cell with a cut off current of $C/20$. After the charge, the cell is stabilized for 1 h and then discharged with a $C/3$ current until the discharge limit voltage is reached. The capacity test shows that the actual maximum capacity of the cell is 2.906 Ah, which is slightly larger than its nominal capacity.

The HPPC test [47] is the most commonly used approach to identify the open circuit voltage and the battery model parameters. The entire HPPC test is composed of several basic cycles, which consist of a single HPPC profile, a constant current discharge to decrease the SOC to a certain value, and a pause for relaxation, as illustrated in Figure 4a,b. The current is assumed positive for discharge and negative for charge here. Each HPPC profile includes a 10-s discharge, a 40-s rest and a 10-s charge, as shown in Figure 4c,d. The unknown parameters of the proposed model can be acquired by minimizing the errors between the predicted voltages and the measured values using a genetic algorithm. The identification results are shown in Table 1. Note that since the parameters are vulnerable to temperature, current rate and cell inconsistency, the offline parameters obtained in this part cannot adapt to all conditions and all cells. Thus, online adjustments are needed.

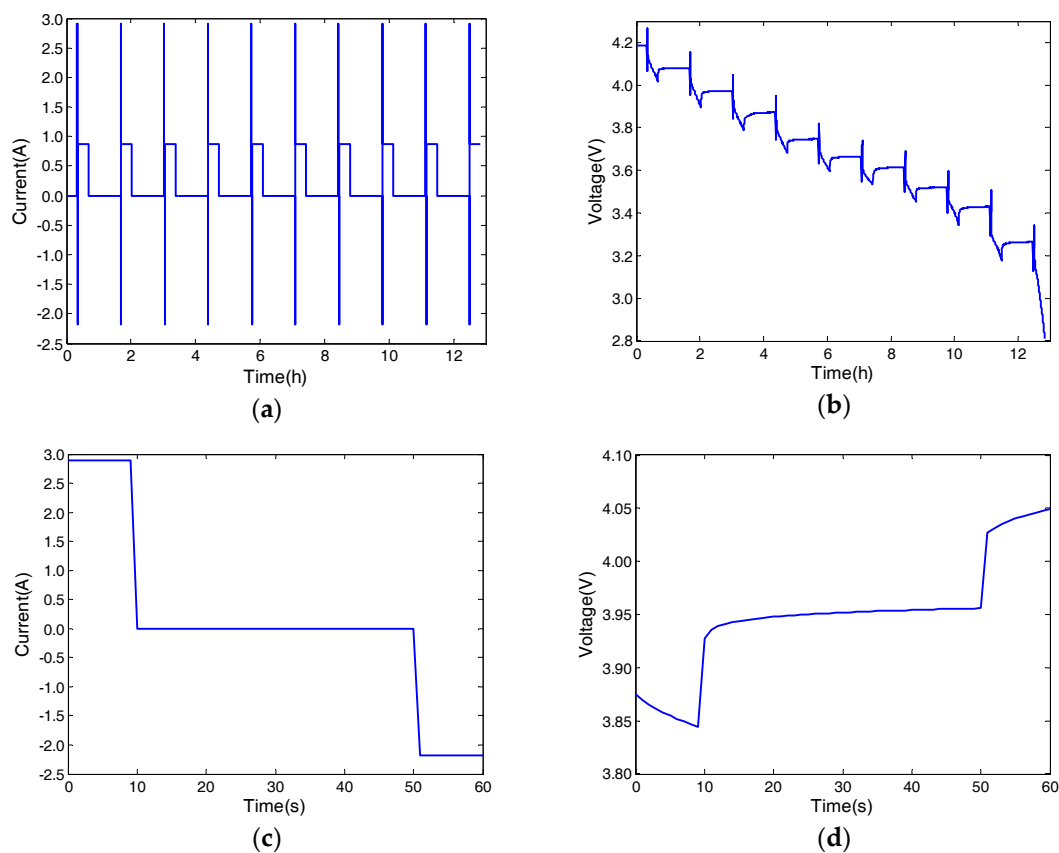


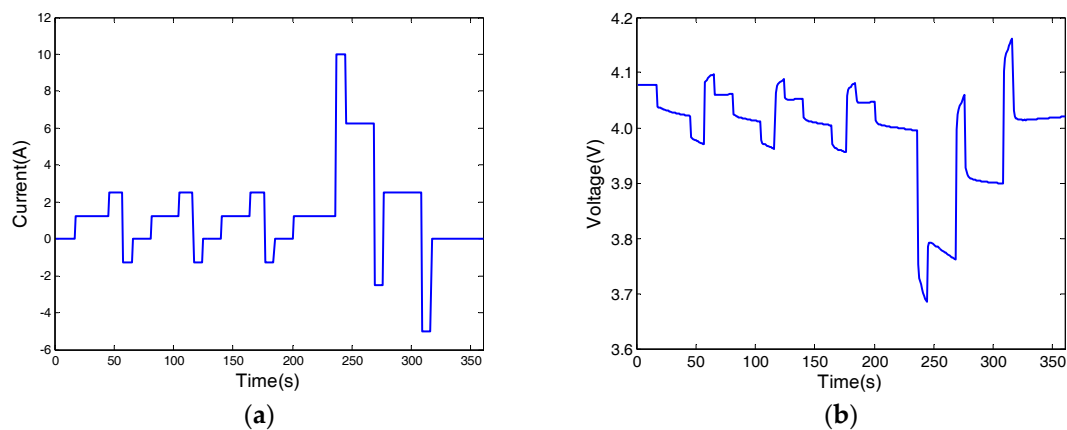
Figure 4. Details of the hybrid pulse power characterization (HPPC) test: (a) current for the entire test; (b) voltage for the entire test; (c) current for one HPPC cycle; and (d) voltage for one HPPC cycle.

Table 1. Model parameter identification results.

Parameter	Value
R_o	0.0384 Ω
R_d	0.0531 Ω
R_e	0.0474 Ω
C_d	2958.6246 F
C_e	29,992.5891 F
α_d	0.9219
α_e	0.8028

5.3. The Dynamic Stress Test

The DST test [48] is a widely used dynamic driving profile to evaluate the performance of the vehicle, and is also used to validate model accuracy or algorithm efficiency [13,49]. In the test, the battery goes through several DST cycles with the SOC operational range from 90% to 20%. The current and voltage profiles of the DST test are shown in Figure 5. To verify the accuracy of the proposed model, the estimated voltages of the entire test are calculated with fixed and variable orders, as shown in Figure 6a. In the fixed-order model, the parameters are extracted from the offline HPPC test, as mentioned above. In the proposed variable-order model, the parameters remain the same as in the fixed model except for the two fractional orders, which will be updated dynamically. For a clearer comparison, the estimation errors are shown in Figure 6b. To verify the efficiency of the proposed SOC estimation method, three algorithms are compared, including the EKF with fixed model, the UKF with fixed model and the UKF with variable model. To verify the robustness of the algorithms, the initial SOCs are adjusted to 100%. The comparative estimation profiles are presented in Figure 6c and their errors are shown in Figure 6d. Additionally, the identification results of the two fractional orders are shown in Figure 6e,f.

**Figure 5.** Details of the dynamic stress test (DST): (a) current and (b) voltage for one DST cycle.

From Figure 6a,b, it can be seen that the fixed model where the parameters are extracted from the offline test cannot accurately track the real data. Conversely, the variable model can capture the voltage response more precisely. Since real time information is considered in the online estimation, the proposed model can achieve more satisfactory results. From Figure 6c,d, it can be seen that the UKF has better estimation accuracy than the EKF. This is because the approximation error from linearization in the EKF is reduced by the unscented transformation method. In addition, the estimated SOC of the variable model follows the reference profile more closely, compared with the fixed model. This proves that the proposed method can improve the SOC estimation accuracy by online adjustment of the model orders. From Figure 6e,f, it can be seen that the fractional orders

vary slowly with time, which intuitively proves that the model orders are dependent on the external operational conditions.

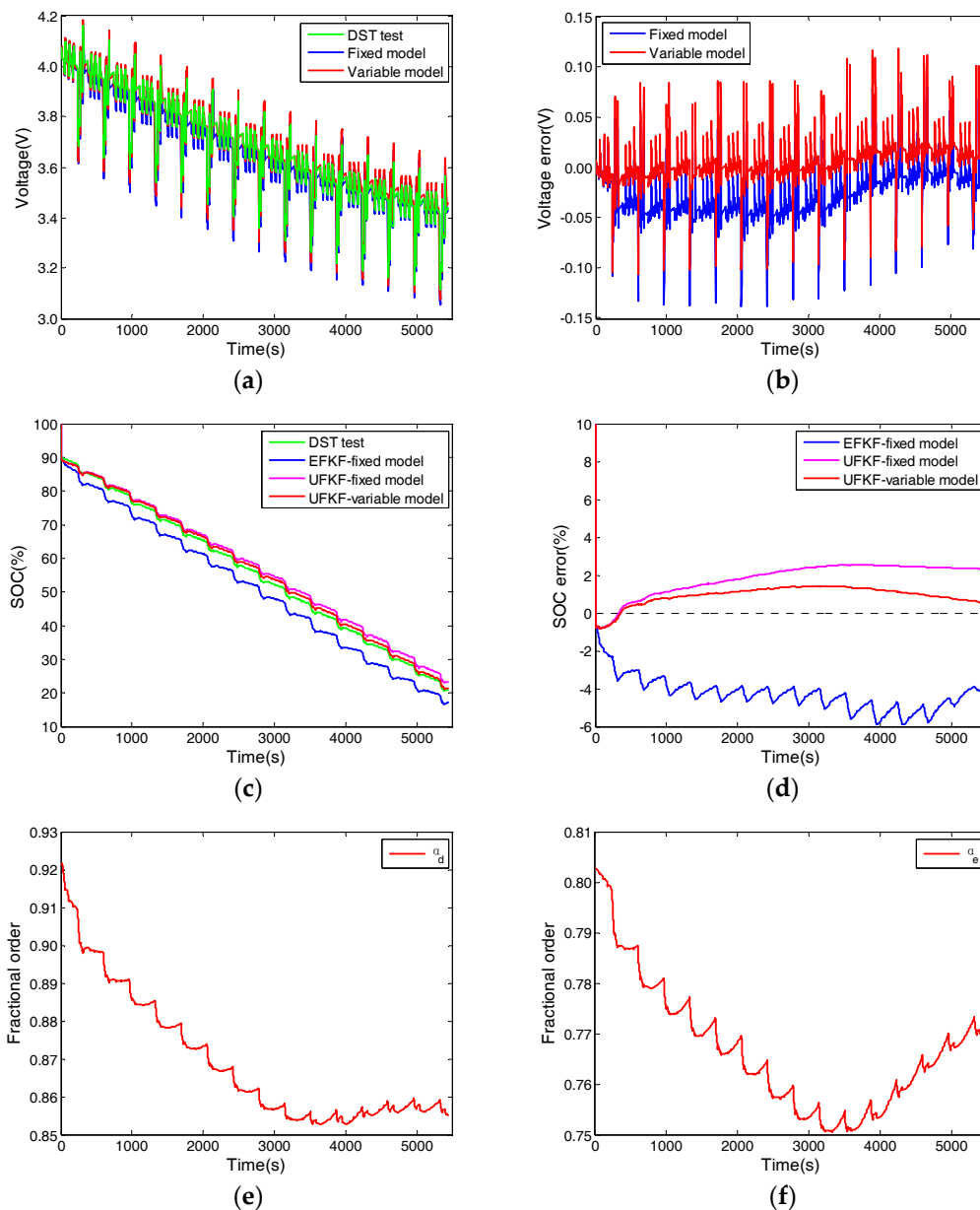


Figure 6. Validation results in the DST: (a) voltage estimation; (b) voltage estimation error; (c) state-of-charge (SOC) estimation; (d) SOC estimation error; (e) evolution of the fractional order α_d and (f) evolution of the fractional order α_e .

5.4. The Federal Urban Dynamic Schedule Test

The FUDS test, which is also called UDDS [50], is another typical dynamic driving cycle to validate the usefulness of models and algorithms [13,51]. Similar to the DST, the battery goes through several FUDS cycles, and the SOC operational range is from 90% to 20%. The current and voltage profiles of the test are shown in Figure 7. The estimated voltages and their errors are shown in Figure 8a,b, respectively. The SOC estimation results with 10% initial error are shown in Figure 8c,d. Finally, the identified orders are shown in Figure 8e,f.

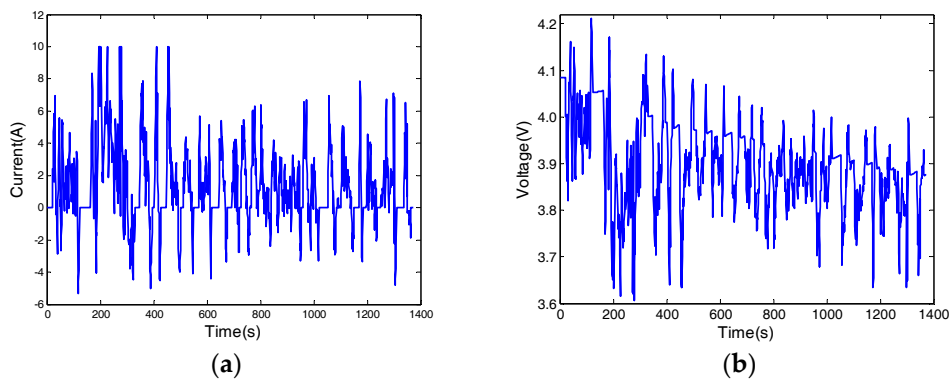


Figure 7. Details of the federal urban dynamic schedule (FUDS) test: (a) current and (b) voltage for one FUDS cycle.

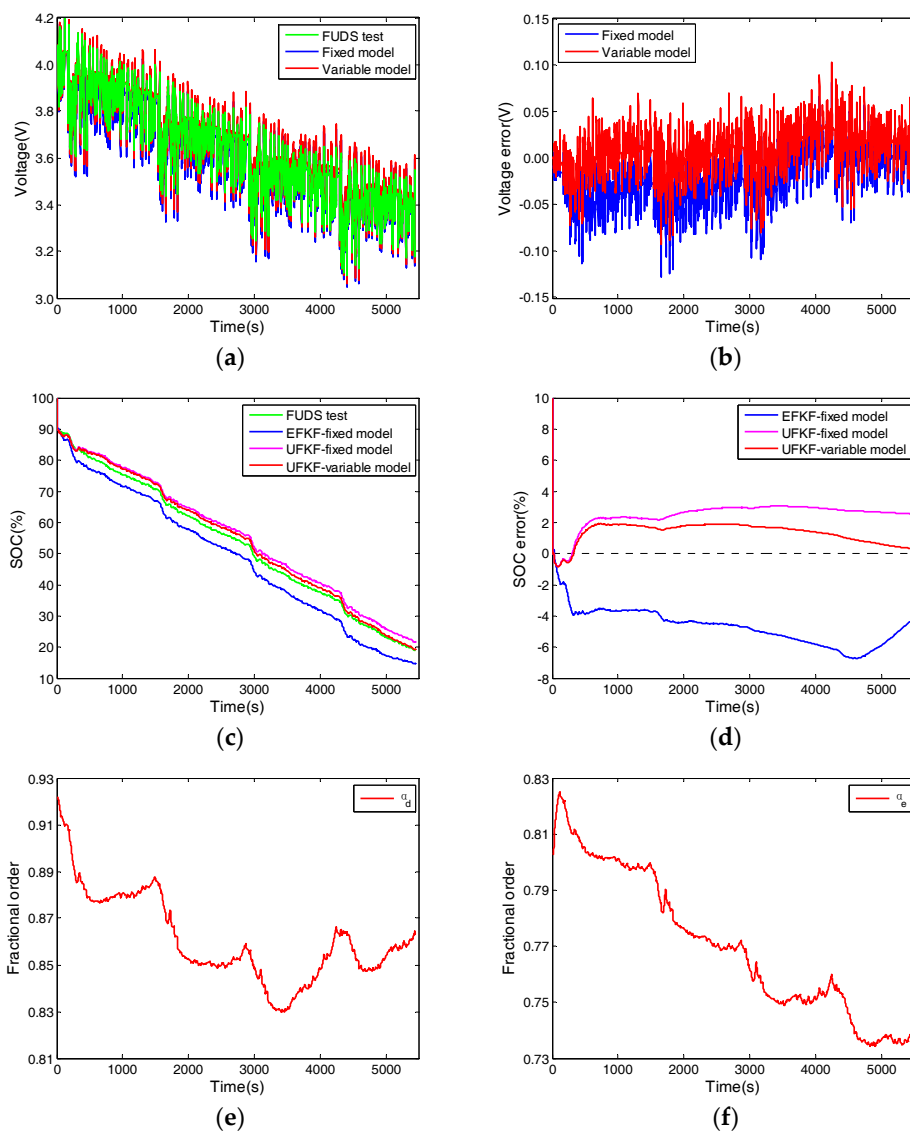


Figure 8. Validation results in the FUDS test: (a) voltage estimation; (b) voltage estimation error; (c) SOC estimation; (d) SOC estimation error; (e) evolution of the fractional order α_d and (f) evolution of the fractional order α_e .

It can be concluded from Figure 8 that the UFKF with variable model has the best performance in terms of both the voltage and SOC estimation. To quantify the superiority of the proposed method, the statistical results are summarized in Tables 2 and 3. For the model accuracy, the root mean square errors (RMSEs) between the estimated voltage and the measured data of the proposed variable model are 19.658 mV in the DST and 21.734 mV in FUDS test, which represent a 45.4% and 42.9% improvement over the fixed parameter models, respectively. The RMSEs for the SOC estimation of the variable model based on the UFKF in the DST and FUDS test are 1.071% and 1.503%, respectively. It should be noted that to emphasize the correction capability of the proposed method, only the two fractional orders are chosen for dual estimation in the tests. The model and SOC accuracy can be further improved by adding a conventional dual filter to update the other model parameters.

Table 2. Comparisons of the RMSE (mV) of the voltage estimation.

Test Profile	Fixed-Order Model	Variable-Order Model
DST	35.970	19.658
FUDS	38.024	21.734

Table 3. Comparisons of the RMSE (%) of the SOC estimation.

Test Profile	EKF with Fixed-Order Model	UFKF with Fixed-Order Model	UFKF with Variable-Order Model
DST	4.379	2.018	1.071
FUDS	4.827	2.590	1.503

6. Conclusions

The fractional order battery models have attracted increasing interest in recent years due to their strong capability to describe battery dynamics. However, since the order values are obtained by offline methods, the accuracy of the existing fractional order models is limited. In addition, the EKF used in the SOC estimation has a number of flaws, such as linearization errors and the complicated computation of the Jacobian matrix. In this paper, three contributions are made. First, a new model with fractional variable-order is proposed. Second, the conventional unscented Kalman filter is implemented for the fractional system and is used for SOC estimation. Third, the dual filter scheme is designed to estimate the SOC and model orders simultaneously. Experimental results show that the variable-order model can precisely simulate the battery dynamics and that the internal SOC can be well estimated using the proposed method.

Acknowledgments: This work is supported by the Science and Technology Planning Project of Guangdong Province (2015B010135006, 2015B010110005) in part, and the Science and Technology Program of Guangzhou (201704020142) in part.

Author Contributions: Xiaojun Tan conceived this paper and designed the experiments; Weijie Chen carried out the experiments and wrote the paper; Ming Cai revised the paper and provided some valuable suggestions.

Conflicts of Interest: The authors declare no conflicts of interest. The founding sponsors had no role in the design of the study; in the collection, analyses, or interpretation of data; in the writing of the manuscript, and in the decision to publish the results.

References

1. Tie, S.F.; Tan, C.W. A review of energy sources and energy management system in electric vehicles. *Renew. Sustain. Energy Rev.* **2013**, *20*, 82–102. [[CrossRef](#)]
2. Kalawoun, J.; Biletska, K.; Suard, F.; Montaru, M. From a novel classification of the battery state of charge estimators toward a conception of an ideal one. *J. Power Sources* **2015**, *279*, 694–706. [[CrossRef](#)]
3. Cuma, M.U.; Koroglu, T. A comprehensive review on estimation strategies used in hybrid and battery electric vehicles. *Renew. Sustain. Energy Rev.* **2015**, *42*, 517–531. [[CrossRef](#)]

4. Li, J.; Klee Barillas, J.; Guenther, C.; Danzer, M.A. A comparative study of state of charge estimation algorithms for lifepo4 batteries used in electric vehicles. *J. Power Sources* **2013**, *230*, 244–250. [[CrossRef](#)]
5. Waag, W.; Fleischer, C.; Sauer, D.U. Critical review of the methods for monitoring of lithium-ion batteries in electric and hybrid vehicles. *J. Power Sources* **2014**, *258*, 321–339. [[CrossRef](#)]
6. Salkind, A.J.; Fennie, C.; Singh, P.; Atwater, T.; Reisner, D.E. Determination of state-of-charge and state-of-health of batteries by fuzzy logic methodology. *J. Power Sources* **1999**, *80*, 293–300. [[CrossRef](#)]
7. Singh, P.; Vinjamuri, R.; Wang, X.; Reisner, D. Design and implementation of a fuzzy logic-based state-of-charge meter for li-ion batteries used in portable defibrillators. *J. Power Sources* **2006**, *162*, 829–836. [[CrossRef](#)]
8. Grewal, S.; Grant, D. A novel technique for modelling the state of charge of lithium ion batteries using artificial neural networks. In Proceedings of the Twenty-Third International Telecommunications Energy Conference, Edinburgh, UK, 14–18 October 2001.
9. Shen, Y. Adaptive online state-of-charge determination based on neuro-controller and neural network. *Energy Convers. Manag.* **2010**, *51*, 1093–1098. [[CrossRef](#)]
10. Anton, J.C.A.; Nieto, P.J.G.; Viejo, C.B.; Vilán, J.A.V. Support vector machines used to estimate the battery state of charge. *IEEE Trans. Power Electron.* **2013**, *28*, 5919–5926. [[CrossRef](#)]
11. Álvarez Antón, J.C.; García Nieto, P.J.; de Cos Juez, F.J.; Sánchez Lasheras, F.; González Vega, M.; Roqueñí Gutiérrez, M.N. Battery state-of-charge estimator using the svm technique. *Appl. Math. Model.* **2013**, *37*, 6244–6253. [[CrossRef](#)]
12. He, H.; Xiong, R.; Guo, H.; Li, S. Comparison study on the battery models used for the energy management of batteries in electric vehicles. *Energy Convers. Manag.* **2012**, *64*, 113–121. [[CrossRef](#)]
13. Hu, X.; Li, S.; Peng, H. A comparative study of equivalent circuit models for li-ion batteries. *J. Power Sources* **2012**, *198*, 359–367. [[CrossRef](#)]
14. Seaman, A.; Dao, T.-S.; McPhee, J. A survey of mathematics-based equivalent-circuit and electrochemical battery models for hybrid and electric vehicle simulation. *J. Power Sources* **2014**, *256*, 410–423. [[CrossRef](#)]
15. Doyle, M.; Fuller, T.F.; Newman, J. Modeling of galvanostatic charge and discharge of the lithium/polymer/insertion cell. *J. Electrochem. Soc.* **1993**, *140*, 1526–1533. [[CrossRef](#)]
16. Fuller, T.F.; Doyle, M.; Newman, J. Simulation and optimization of the dual lithium ion insertion cell. *J. Electrochem. Soc.* **1994**, *141*, 1–10. [[CrossRef](#)]
17. Smith, K.A.; Rahn, C.D.; Wang, C.-Y. Model-based electrochemical estimation and constraint management for pulse operation of lithium ion batteries. *IEEE Trans. Control Syst. Technol.* **2010**, *18*, 654–663. [[CrossRef](#)]
18. Ashwin, T.R.; McGordon, A.; Widanage, W.D.; Jennings, P.A. Modified electrochemical parameter estimation of ncr18650bd battery using implicit finite volume method. *J. Power Sources* **2017**, *341*, 387–395. [[CrossRef](#)]
19. Liaw, B.Y.; Nagasubramanian, G.; Jungst, R.G.; Doughty, D.H. Modeling of lithium ion cells—A simple equivalent-circuit model approach. *Solid State Ion.* **2004**, *175*, 835–839.
20. Plett, G.L. Extended kalman filtering for battery management systems of lipb-based hev battery packs. *J. Power Sources* **2004**, *134*, 262–276. [[CrossRef](#)]
21. He, H.; Xiong, R.; Fan, J. Evaluation of lithium-ion battery equivalent circuit models for state of charge estimation by an experimental approach. *Energies* **2011**, *4*, 582–598. [[CrossRef](#)]
22. Sierociuk, D.; Dzielinski, A.; Sarwas, G.; Petras, I.; Podlubny, I.; Skovranek, T. Modelling heat transfer in heterogeneous media using fractional calculus. *Philos. Trans. R. Soc. A* **2013**, *371*, 20120146. [[CrossRef](#)] [[PubMed](#)]
23. Freeborn, T.J. A survey of fractional-order circuit models for biology and biomedicine. *IEEE J. Emerg. Sel. Top. Circuits Syst.* **2013**, *3*, 416–424. [[CrossRef](#)]
24. Wu, H.; Yuan, S.; Yin, C. A lithium-ion battery fractional order state space model and its time domain system identification. In *Proceedings of the FISITA 2012 World Automotive Congress*; Springer: Berlin, Germany, 2013; pp. 795–805.
25. Wang, B.; Li, S.E.; Peng, H.; Liu, Z. Fractional-order modeling and parameter identification for lithium-ion batteries. *J. Power Sources* **2015**, *293*, 151–161. [[CrossRef](#)]
26. Zou, Y.; Li, S.E.; Shao, B.; Wang, B. State-space model with non-integer order derivatives for lithium-ion battery. *Appl. Energy* **2016**, *161*, 330–336. [[CrossRef](#)]
27. Wang, B.; Liu, Z.; Li, S.E.; Moura, S.J.; Peng, H. State-of-charge estimation for lithium-ion batteries based on a nonlinear fractional model. *IEEE Trans. Control Syst. Technol.* **2017**, *25*, 3–11. [[CrossRef](#)]

28. Zhong, F.; Li, H.; Zhong, S.; Zhong, Q.; Yin, C. An soc estimation approach based on adaptive sliding mode observer and fractional order equivalent circuit model for lithium-ion batteries. *Commun. Nonlinear Sci. Numer. Simul.* **2015**, *24*, 127–144. [[CrossRef](#)]
29. Liu, C.; Liu, W.; Wang, L.; Hu, G.; Ma, L.; Ren, B. A new method of modeling and state of charge estimation of the battery. *J. Power Sources* **2016**, *320*, 1–12. [[CrossRef](#)]
30. Xu, J.; Mi, C.C.; Cao, B.; Cao, J. A new method to estimate the state of charge of lithium-ion batteries based on the battery impedance model. *J. Power Sources* **2013**, *233*, 277–284. [[CrossRef](#)]
31. Xiao, R.; Shen, J.; Li, X.; Yan, W.; Pan, E.; Chen, Z. Comparisons of modeling and state of charge estimation for lithium-ion battery based on fractional order and integral order methods. *Energies* **2016**, *9*, 184. [[CrossRef](#)]
32. Yu, W.; Luo, Y.; Pi, Y. Fractional order modeling and control for permanent magnet synchronous motor velocity servo system. *Mechatronics* **2013**, *23*, 813–820. [[CrossRef](#)]
33. Hajiloo, A.; Nariman-zadeh, N.; Moeini, A. Pareto optimal robust design of fractional-order pid controllers for systems with probabilistic uncertainties. *Mechatronics* **2012**, *22*, 788–801. [[CrossRef](#)]
34. Gabano, J.-D.; Poinot, T. Fractional identification algorithms applied to thermal parameter estimation. *IFAC Proc. Vol.* **2009**, *42*, 1316–1321. [[CrossRef](#)]
35. Narang, A.; Chen, T.; Shah, S.L. Continuous-time model identification of fractional-order models with time delays. *IET Control Theory Appl.* **2011**, *5*, 900–912. [[CrossRef](#)]
36. Podlubny, I. *Fractional Differential Equations: An Introduction to Fractional Derivatives, Fractional Differential Equations, to Methods of Their Solution and Some of Their Applications*; Academic Press: San Diego, CA, USA, 1998; Volume 198.
37. Monje, C.A.; Chen, Y.; Vinagre, B.M.; Xue, D.; Feliu-Batlle, V. *Fractional-Order Systems and Controls: Fundamentals and Applications*; Springer Science & Business Media: London, UK, 2010.
38. Sierociuk, D.; Macias, M.; Malesza, W.; Sarwas, G. Dual estimation of fractional variable order based on the unscented fractional order kalman filter for direct and networked measurements. *Circuits Syst. Signal Process.* **2016**, *35*, 2055–2082. [[CrossRef](#)]
39. Hasan, R.; Scott, J.B. Fractional behaviour of rechargeable batteries. In Proceedings of the 2016 Electronics New Zealand Conference (ENZCon 2016), Wellington, New Zealand, 17–18 November 2016; Electronics New Zealand Inc.: Hamilton, New Zealand, 2016; pp. 111–114.
40. Sadli, I.; Urbain, M.; Hinaje, M.; Martin, J.-P.; Raël, S.; Davat, B. Contributions of fractional differentiation to the modelling of electric double layer capacitance. *Energy Convers. Manag.* **2010**, *51*, 2993–2999. [[CrossRef](#)]
41. Samadani, E.; Farhad, S.; Scott, W.; Mastali, M.; Gimenez, L.E.; Fowler, M.; Fraser, R.A. Empirical modeling of lithium-ion batteries based on electrochemical impedance spectroscopy tests. *Electrochim. Acta* **2015**, *160*, 169–177. [[CrossRef](#)]
42. Swamy, T.; Chiang, Y.-M. Electrochemical charge transfer reaction kinetics at the silicon-liquid electrolyte interface. *J. Electrochem. Soc.* **2015**, *162*, A7129–A7134. [[CrossRef](#)]
43. Caballero-Aguila, R.; Hermoso-Carazo, A.; Linares-Pérez, J. Extended and unscented filtering algorithms in nonlinear fractional order systems with uncertain observations. *Appl. Math. Sci.* **2012**, *6*, 1471–1486.
44. He, H.; Xiong, R.; Guo, H. Online estimation of model parameters and state-of-charge of lifepo4 batteries in electric vehicles. *Appl. Energy* **2012**, *89*, 413–420. [[CrossRef](#)]
45. Zhang, L.; Wang, Z.; Sun, F.; Dorrell, D. Online parameter identification of ultracapacitor models using the extended kalman filter. *Energies* **2014**, *7*, 3204–3217. [[CrossRef](#)]
46. Zhou, D.; Zhang, K.; Ravey, A.; Gao, F.; Miraoui, A. Parameter sensitivity analysis for fractional-order modeling of lithium-ion batteries. *Energies* **2016**, *9*, 123. [[CrossRef](#)]
47. Belt, J.R. *Battery Test Manual for Plug-In Hybrid Electric Vehicles*; Idaho National Laboratory (INL): Idaho Falls, ID, USA, 2010.
48. USCAR. Manuals: Electric Vehicle Battery Test Procedures Manual. Available online: <http://www.uscar.org/guest/publications> (accessed on 30 August 2017).
49. Robertson, D.C.; Christophersen, J.P.; Bennett, T.; Walker, L.K.; Wang, F.; Liu, S.; Fan, B.; Bloom, I. A comparison of battery testing protocols: Those used by the us advanced battery consortium and those used in china. *J. Power Sources* **2016**, *306*, 268–273. [[CrossRef](#)]

50. EPA Urban Dynamometer Driving Schedule (UDDS). Available online: <https://www.epa.gov/emission-standards-reference-guide/epa-urban-dynamometer-driving-schedule-udds> (accessed on 30 August 2017).
51. Xiong, R.; Sun, F.; Gong, X.; He, H. Adaptive state of charge estimator for lithium-ion cells series battery pack in electric vehicles. *J. Power Sources* **2013**, *242*, 699–713. [[CrossRef](#)]



© 2017 by the authors. Licensee MDPI, Basel, Switzerland. This article is an open access article distributed under the terms and conditions of the Creative Commons Attribution (CC BY) license (<http://creativecommons.org/licenses/by/4.0/>).